

Muon Acceleration for Neutrino Factory

V. Lebedev, *Jefferson Lab, Newport News, VA 23693*

A concept for a neutrino factory muon accelerator driver is presented. Acceleration of a muon beam is a challenging task because of a large source phase space and short species lifetime. In the design concept presented here, acceleration starts after ionization cooling at 210 MeV/c and proceeds to 20 GeV where the beam is injected into a neutrino factory storage ring. The key technical issues, beyond the basic physics parameters of Table 1, are: 1) choice of acceleration technology (superconducting versus normal conducting cavities) and related to it RF frequency choice, 2) choice of acceleration scheme, 3) capture, acceleration, transport and preservation of the large source phase space of the fast decaying species, and 4) accelerator performance issues such as potential collective effects (e.g., cumulative beam breakup) resulting from the high peak current. To counteract muon decay the highest possible accelerating gradient is required. That is the major driver for the proposed scheme. The muon accelerator driver (MAD) consists of a 2.87 GeV linac and consecutive four-pass recirculating linear accelerator as shown in Figure 1.

Table 1. Main Parameters of the Muon Accelerator Driver

Injection momentum/Kinetic energy	210/129.4 MeV
Final energy	20 GeV
Initial normalized acceptance	15 mm·rad
rms normalized emittance	2.4 mm·rad
Initial longitudinal acceptance, $\Delta p L_b / m_\mu$	170 mm
momentum spread, $\Delta p/p$	± 0.21
bunch length, L_b	± 407 mm
rms energy spread	0.084
rms bunch length	163 mm
Number of bunches per pulse	67
Number of particles per bunch/per pulse	$4.4 \cdot 10^{10} / 3 \cdot 10^{12}$
Bunch frequency/accelerating frequency	201.25/201.25 MHz
Average repetition rate	15 Hz
Time structure of muon beam	6 pulses at 50 Hz with 2.5 Hz repetition rate
Average beam power	150 kW

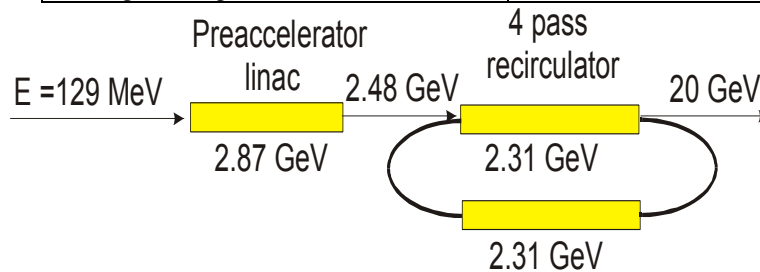


Figure 1. Layout of the muon accelerator driver

Very large transverse and longitudinal accelerator acceptances drive the design to low RF frequency. Were normal-conducting cavities used, the required high gradients of order of ~ 15 MV/m would demand unachievably high peak power of RF sources. Superconducting RF (SRF) cavities are a much more attractive solution. RF power can then be delivered to the cavities over an extended time, and thus RF source peak power can be reduced. Another important advantage of SRF cavities is that their design is not limited by a requirement of low shunt impedance and therefore their aperture can be significantly larger. Taking into account the required longitudinal and transverse acceptances and that the beam is already bunched at 201.25 MHz at the source (ionization cooling) the 201.25 MHz RF-frequency has been chosen for both the linear accelerator and the recirculator. This choice also provides adequate stored energy to accelerate multiple passes of a single-pulse bunch train without need to refill the extracted energy between turns.

Muon survival practically excludes use of conventional circular accelerator and demands either a high-gradient conventional or recirculating linac. While recirculation provides significant cost savings over a single linac, it cannot be utilized at low energy for two reasons. First, at low energy the beam is not sufficiently relativistic and will therefore cause a phase slip for beams in higher passes, thus significantly reducing acceleration efficiency for subsequent passes. Secondly, there are major difficulties associated with injection of a beam with the large emittance and energy spread associated with a muon source. Beam pre-acceleration in a linear accelerator to about 2.5 GeV makes the beam sufficiently relativistic and adiabatically decreases the phase space volume so that further acceleration in recirculating linacs is possible.

Cost considerations favor multiple passes per stage, but practical experience commissioning and operating recirculating linacs dictates prudence. Experience at Jefferson Lab suggests that for

given large initial emittance and energy spread, a ratio of final-to-injected energy below 10-to-1 is prudent and the number of passes should be limited to about five¹. We therefore propose a machine architecture (see Figure 1) featuring a 0.13-to-2.48 GeV straight “preaccelerator” linac, and 2.48-to-20 GeV four pass recirculating linac (RLA). Figure 2 shows loss of muons in the course of acceleration. One can see that although RLA gives significant contribution the major fraction comes from the linac. One can also

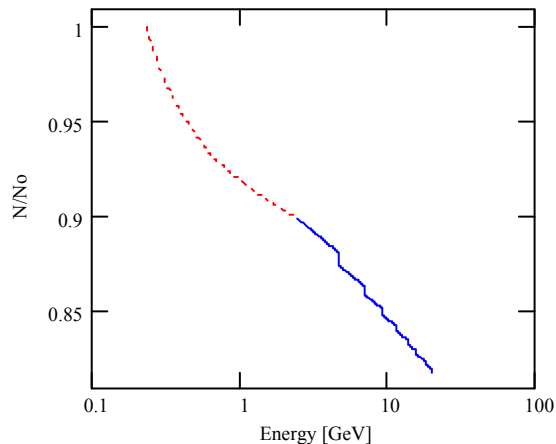


Figure 2. Decay of muons in the course of acceleration; dotted line – decay in the linac, solid line – decay in the recirculator. Vertical drops correspond to the beam transport in arcs.

¹ Note that for given parameters further increase of number of passes reduces effective accelerating gradient and consequently leads to higher decay of muons.

see that arcs (vertical drops in Figure 2) do not contribute much in the decay, which justifies the choice of normal conducting bends, and triplet focusing discussed below.

1. Linear accelerator

1.1 Linac general parameters and lattice period layout

Initial large acceptance of the accelerator requires large aperture and tight focusing at its front-end. In the case of large aperture, tight space, moderate energy and necessity of strong focusing in both planes the solenoidal focusing is superior to the triplet focusing and has been chosen for the entire linac. To achieve a manageable beam size at the linac front-end short focusing cells are used for the first 11 cryo-modules. The beam size is adiabatically damped with acceleration, and that allows one to replace short cryo-modules with intermediate-length cryo-modules and then, when the energy reaches 0.75 GeV by long (standard) cryo-modules. In comparison with the standard 13 m cryo-modules the short and intermediate-length cryo-modules have increased aperture and, consequently, reduced accelerating gradient. Main parameters of the linac and its periods are presented in Tables 2 and 3. Figure 3 depicts the layouts of short, intermediate-length and long cryo-modules. Figures 4 and 5 present the beam envelope and beta-function along the linac.

Table 2. Main parameters of linear accelerator

Injection momentum/Kinetic energy	210 / 129.4 MeV
Final momentum/Kinetic energy	2583 / 2480 MeV
Total linac length	433 m
Acceptance: initial / final (no emittance dilution)	7.5 / 0.62 mm-rad
Momentum spread: initial / final	$\pm 0.21 / \pm 0.075$
Total bunch length: initial / final	814 / 190 mm 197 / 46 deg
Total installed accelerating voltage	2.87 GeV

Table 3. Parameters of the long and short periods of linear accelerator

	Short cryo-module	Intermediate-length cryo-module	Long cryo-module
Number of periods	11	16	19
Total length of one period	5 m	8 m	13 m
Number of cavities per period	1	2	4
Number of cells per cavity	2	2	2
Number of couplers per cavity	2	2	2
Cavity accelerating gradient	15 MV/m	15 MV/m	17 MV/m
Real-estate gradient	4.47 MV/m	5.59 MV/m	7.79 MV/m
Aperture in cavities ($2a$)	460 mm	460 mm	300 mm
Aperture in solenoids ($2a$)	460 mm	460 mm	360 mm
Solenoid length	1 m	1 m	1.5 m
Solenoid maximum field	2.1 T	2.1 T	4.2 T

The layout of cryo-modules and the arrangement of SC cavities are determined by the requirement to keep power of the fundamental coupler at acceptable level and to have cavities sufficiently decoupled. The coupler power limitation (below 1 MW) requires 1 coupler per cell and therefore we choose to have the coupler at each side of two-cell

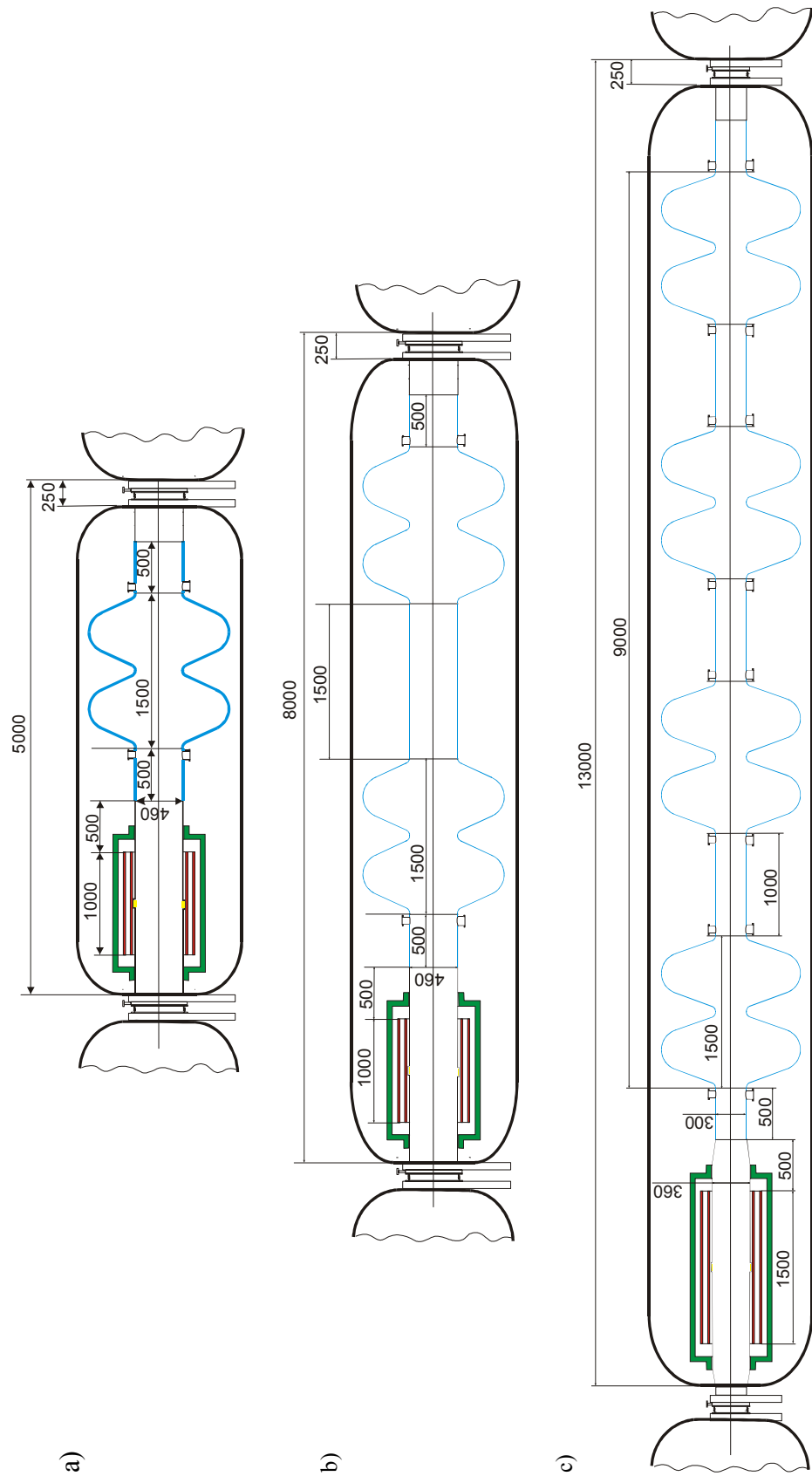


Figure 3. Layouts of a) short, b) intermediate-length, and c) long cryo-modules. Blue lines present SC walls of cavities. Solenoid coils are marked by red color, and BPMs by the yellow.

Fri Feb 23 10:42:26 2001 OptiM - MAIN: - C:\Optics\NeutrinoFactory\Linac\Linac.opt

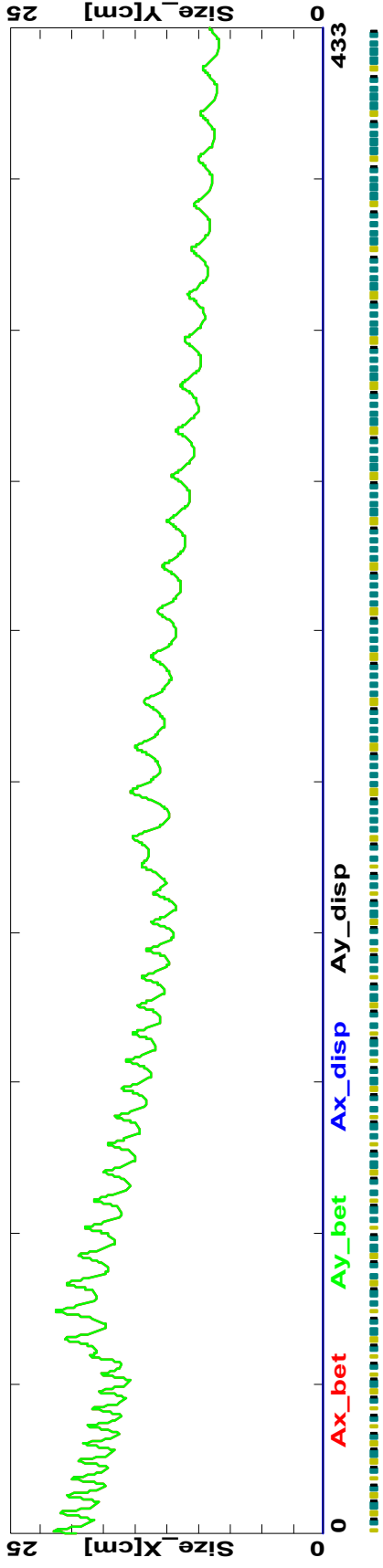


Figure 4. Beam envelopes of the entire beam (2.5σ) along linear accelerator

Fri Feb 23 10:40:52 2001 OptiM - MAIN: - C:\Optics\NeutrinoFactory\Linac\Linac.opt

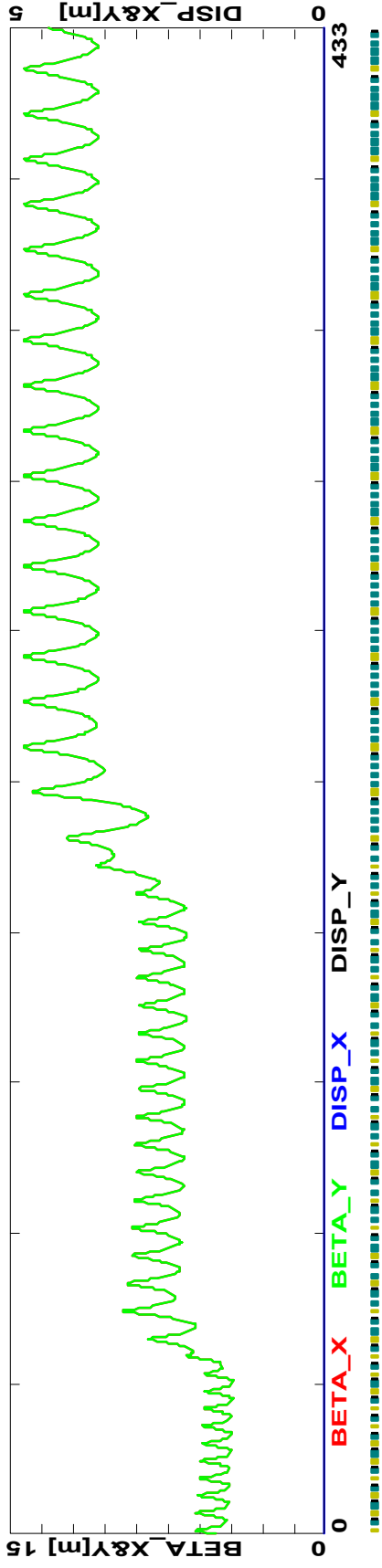


Figure 5. Beta-functions along the linear accelerator. The beta-functions are computed in the frame, which rotates with angular frequency equal to $\omega = eB_s/2pc$ so that the beam motion would be decoupled.

cavity.

The coupling coefficient determined as $\delta = C_3 / C_1$ (see Figure 6) should be sufficiently small,

$$\delta \leq \frac{1}{10Q}, \quad (1)$$

to have a possibility to by-pass not properly functioning cavities. Figure 7 demonstrates effects of cavity coupling and detuning on the cavity voltage. Thus for loaded Q of $5 \cdot 10^5$ the required cavity decoupling should be below $2 \cdot 10^{-6}$.

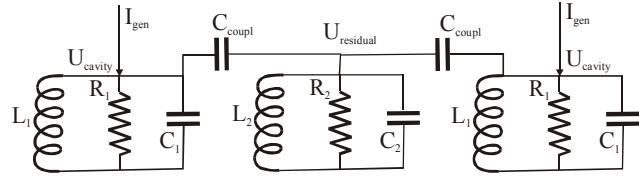


Figure 6. Electrical circuitry for calculation of cavity coupling

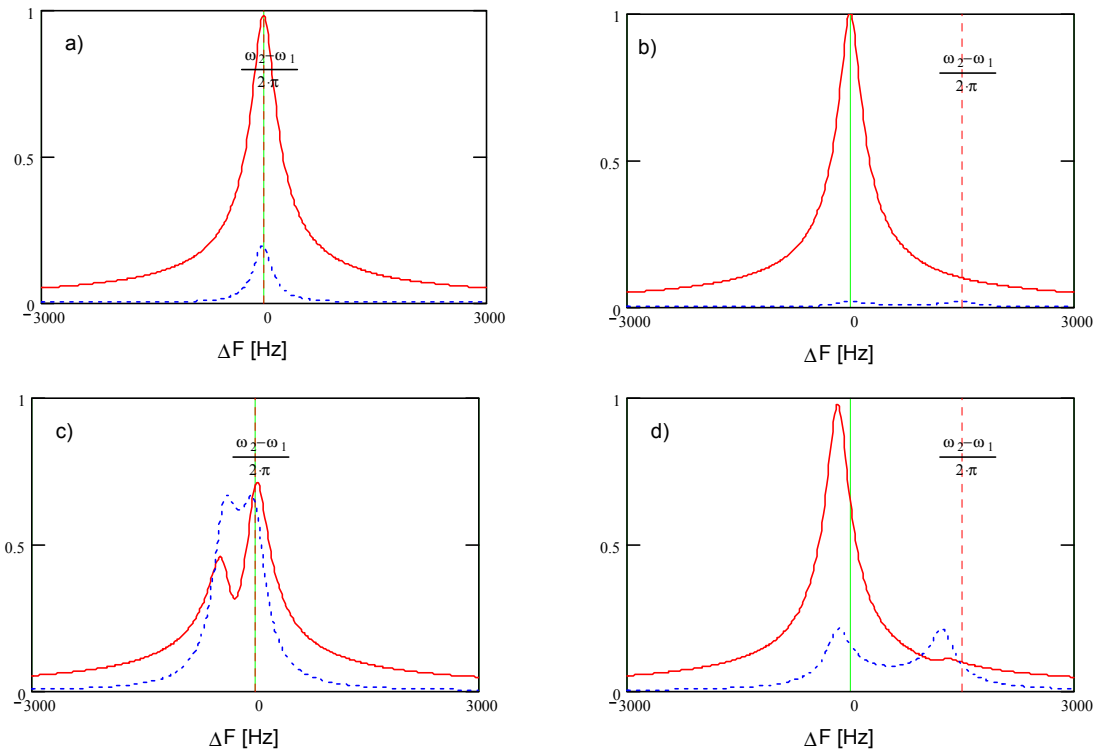


Figure 7. Dependence of cavity voltage on frequency. Solid lines – voltage for normally powered cavity; dashed line – voltage for not properly functioning cavity with corresponding power generator off; a)&c) - cavity is not detuned, b)&d) - cavity is detuned by five bandwidth; a)&b) $\delta = 0.1 / Q$, c)&d) $\delta = 1 / Q$; $Q = 5 \cdot 10^5$.

Such decoupling requires significant distances between nearby cavities. For an estimate one can assume that coupling between cavity cells to be 5%, and then using results presented in Figure 8 one obtains that distance between cavities has to be more than 110 cm for short cry-modules and 70 cm for long cryo-modules. Taking into account that the fundamental and high HOM couplers are located in the same space these distances were chosen to be 150 and 100 cm, correspondingly. BPMs are located inside solenoids to reduce effects of EMI signals coming from RF cavities

There is an additional limitation on the layout of the linac determined by a requirement that all cavities are treated and vacuumed in a clean room and kept under

vacuum all the time after it. That determines that each cryo-module has to have vacuum valves at both ends with corresponding transition modules from liquid helium temperature to the room temperature. To achieve the maximum real-estate accelerating gradient the focusing solenoids are also located inside cryo-modules.

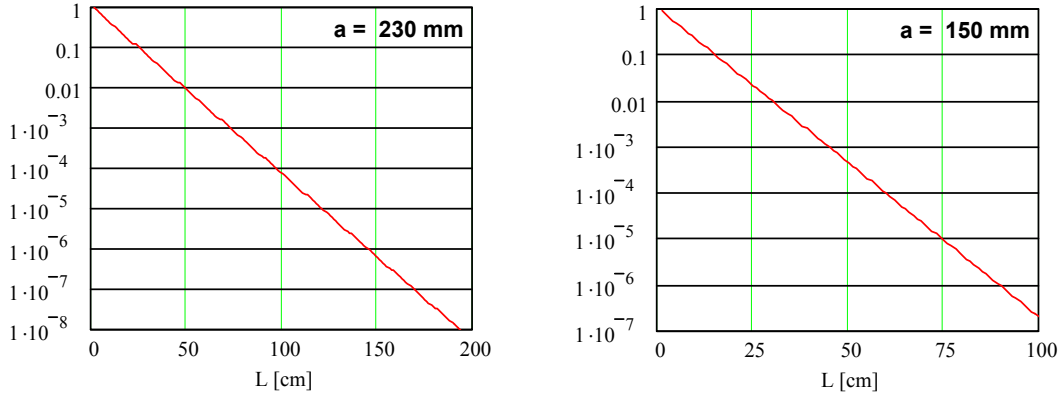


Figure 8. Attenuation of the electromagnetic wave between two cavities for short (left) and long (right) cryo-modules. The attenuation is estimated by the following formula: $\delta = \exp\left(-L\sqrt{(\mu_0/a)^2 - (2\pi/\lambda)^2}\right)$.

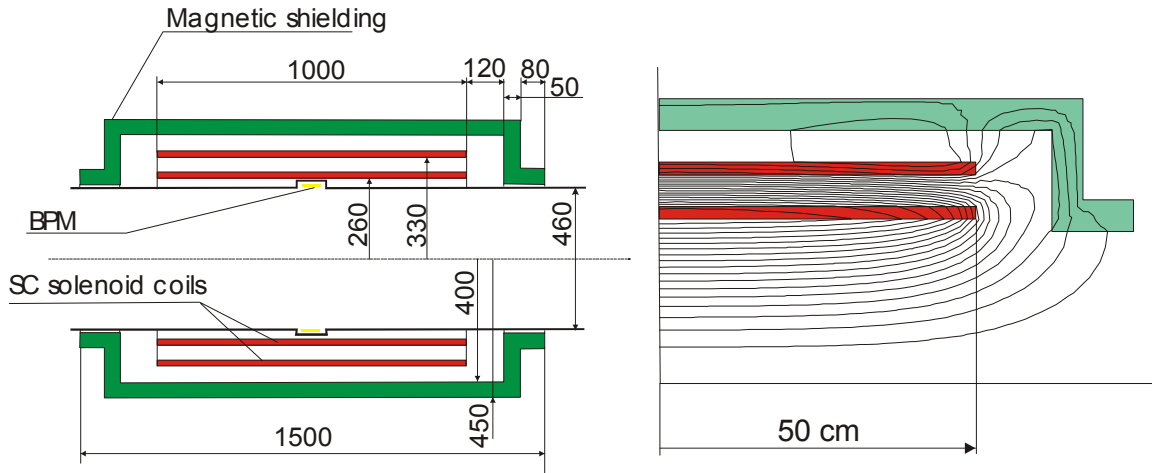


Figure 9. Layout of short solenoid and plot of its magnetic lines

Taking the large aperture required by the beam size the question of solenoids focusing linearity has to be addressed. The dependence of focusing strength on radius can be approximated by the following expression:

$$\Phi \equiv \frac{1}{F} \approx \left(\frac{e}{2pc}\right)^2 \left(\int B^2 ds + \frac{r^2}{2} \int B'^2 ds \right) \approx L \left(\frac{eB_0}{2pc}\right)^2 \left(1 + \frac{r^2}{3aL}\right) \quad (2)$$

where L and a are the solenoid length and radius. As one can see from Eq. (2) to reduce the non-linearity one needs to increase the solenoid length and aperture. Increasing length directly decreases the real-estate gradient; while increasing aperture requires larger distance between the solenoid and cavity to shield magnetic field and in the final score also decreases real-estate gradient. Aperture increase also makes solenoids more

expensive and less reliable. The length of short solenoid has been chosen to be 1 m as a compromise between these contradictory requirements. The length of long solenoids is determined by the magnetic field limitation and is chosen to be 1.5 m. The layout of the short solenoid and plots of magnetic lines are shown in Figure 9. To achieve fast field drop from solenoid to cavity the solenoid has an outer counter-coil, which intercepts its magnetic flux, and the cavity has a SC shielding at its outer surface. That allows one to achieve magnetic field less than 0.1 G inside the cavity as depicted in Figure 10.

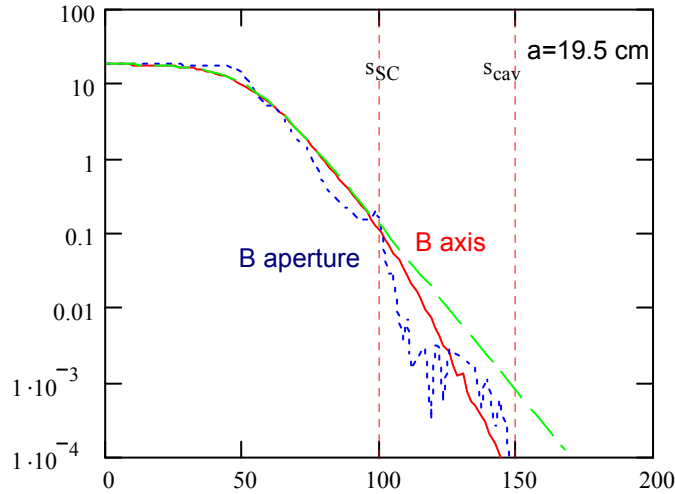


Figure 10. Dependence of magnetic field on longitudinal coordinate: solid line - on the axis, dotted line - on the radius equal to the cavity radius of 23 cm, dashed line - fitting with the following formula: $B(s) = (B_0 / 2)(1 - \tanh((s - L / 2) / a))$, where $a = 19.5$ cm. Vertical lines show positions where the SC screen and cavity start.

1.2 Longitudinal beam dynamics

Initial bunch length and energy spread are very large, so that the bunch length is more than the half wave length ($\Delta\phi = \pm 89$ deg) and the momentum acceptance is about $\pm 21\%$. Therefore their decrease (due to adiabatic damping) to a manageable level is the most important assignment of the beam acceleration in the linac. The final linac energy is also determined by achieving velocity sufficiently close to the light velocity so that there would not be significant RF phase slip for higher passes in the recirculator.

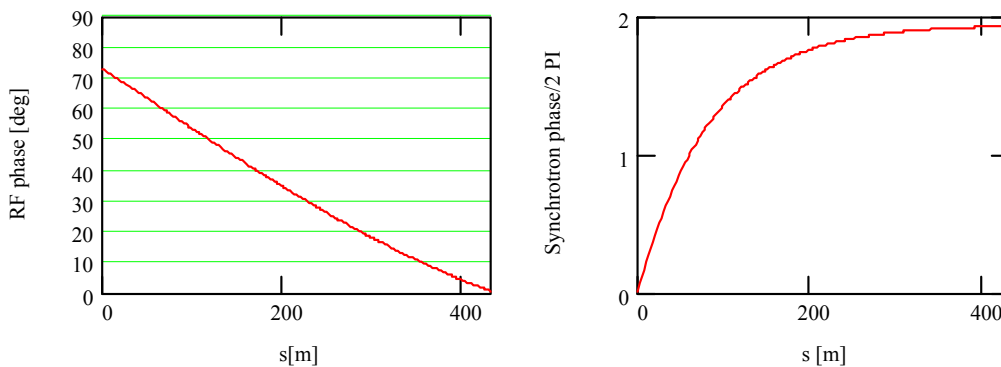


Figure 11. RF (left) and synchrotron (right) phases along the linac.

To perform adiabatic bunching, the RF phase of the cavities is shifted by 73 deg at

the beginning of the linac and is gradually changed to zero at the linac end as shown in Figure 11. In the first half of the linac, when the beam is still not sufficiently relativistic, the offset causes synchrotron motion which prevents the sag in acceleration for the bunch head and tail, and allows bunch compression in both length and momentum spread to $\Delta p/p = \pm 7.5\%$ and $\Delta\phi = \pm 23$ deg but the RF phase offset also reduces effective accelerating gradient so that the total voltage of 2.87 GV is required for the beam acceleration of 2.35 GeV. To maximize longitudinal acceptance its initial position is shifted relative to the center of the bucket. Figure 12 depicts position of the beam boundary inside separatrix; and Figure 13 shows how the initially elliptical boundary of the bunch longitudinal phase space is transformed to the end of the linac.

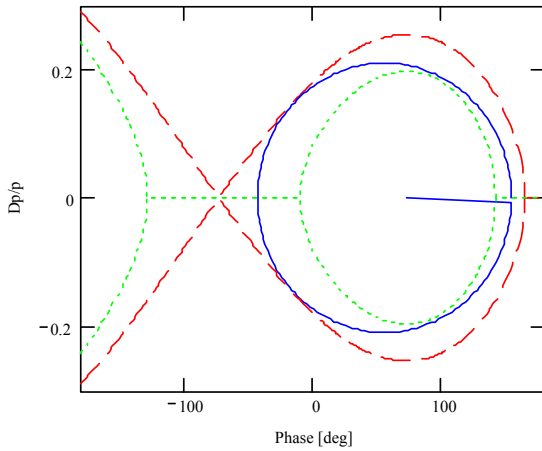


Figure 12. Beam boundary (solid line) inside separatrix (dashed line) shown at the beginning of the linac.

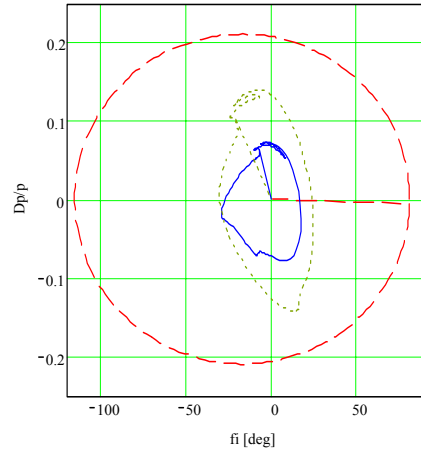


Figure 13. Beam boundary at the beginning (dashed line), in the middle (dotted line) (left) and at the end of the linac

1.3 Transverse beam dynamics and tracking

Betatron phase advance per cell, ν , is important parameter determining properties of the beam transport in the linac. There are a few considerations, which need to be taken into account. First, large beam emittance and limited aperture in the cavities require minimization of the beam size for a given period length. As one can see from Figure 14 it points to ν close to 0.25. Second, one would like to minimize dependence of beta-function variation with momentum. For the same initial conditions the beta-function oscillates relative to its nominal value if momentum is changed. Figure 15 presents ratio of maximum beta-function achieved in the course of oscillations to the maximum of beta-function at equilibrium energy. As one can see for momentum spread of $\pm 20\%$ it requires tunes below 0.25. Third, solenoids are short comparative to the beam aperture

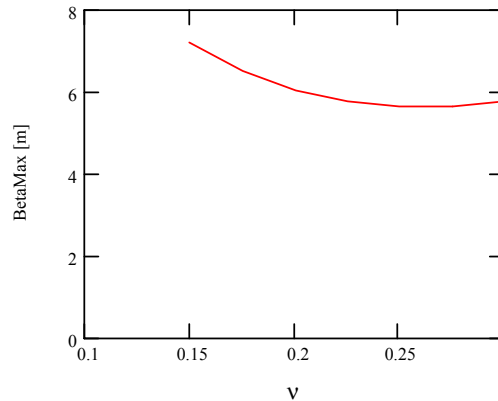


Figure 14. Dependence of maximum beta-function on tune advance per cell for a line with solenoidal focusing and period length 6 m.

and therefore they have significant non-linearity in their focusing. As one can see from Eq. (2) for $a = 19$ cm, $r = 23$ cm and $L=1$ m one obtains correction of focusing strength of 9% at the beam boundary. Such non-linearity can cause strong non-linear resonance even for small number of lattice periods. Figure 16 presents how beam emittance is changing for different phase advances per cell after passing a channel with 50 solenoidal lenses. One can see very strong effect of the $1/4$ resonance which spreads in the tune range of $[0.21 - 0.24]$. The $1/6$ resonance is also well visible but does not produce so harmful effect. In reality it is much smaller because of adiabatic damping of the beam size with acceleration. Taking all above into account we choose tune to be equal to 0.175.

Particle distribution for tracking has been chosen to be Gaussian in 6D phase space but the tails of the distribution are truncated at 2.5σ , which corresponds to the beam acceptance presented in Table 1. Despite the large initial energy spread, particle tracking through the linac does not exhibit any significant emittance growth with 0.2% beam loss coming mainly from particles at the longitudinal phase space boundary. Figure 17 presents longitudinal phase space at the beginning and the end of accelerator. Figure 18 shows the beam emittances and beam envelopes and beam intensity along the linac. Sudden increase and then decrease of the envelopes correspond to a particle motion instability with consecutive particle scraping. The decay of muons is not taken into account in the beam intensity plot.

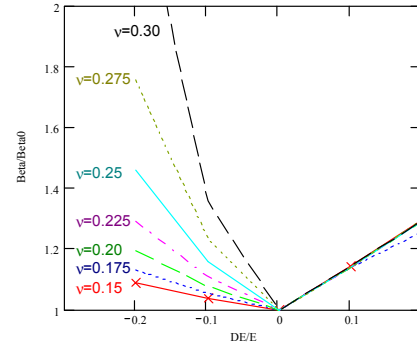


Figure 15. Dependence of relative change of beta-function maximum on relative momentum change for different tune advances per cell.

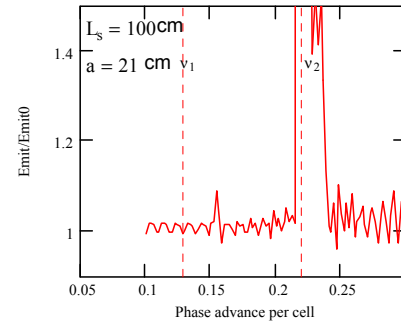


Figure 16. Relative emittance change after passing 50 solenoidal lenses of 1 m length; $\epsilon_n = 15$ mm rad, vertical lines show betatron tune spread in the beam: $\Delta v/v \approx \Delta p/p = \pm 26\%$

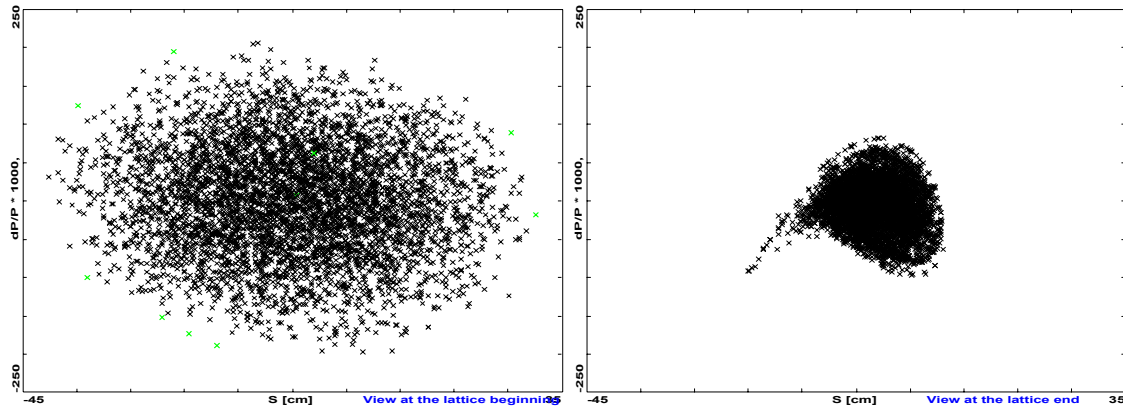
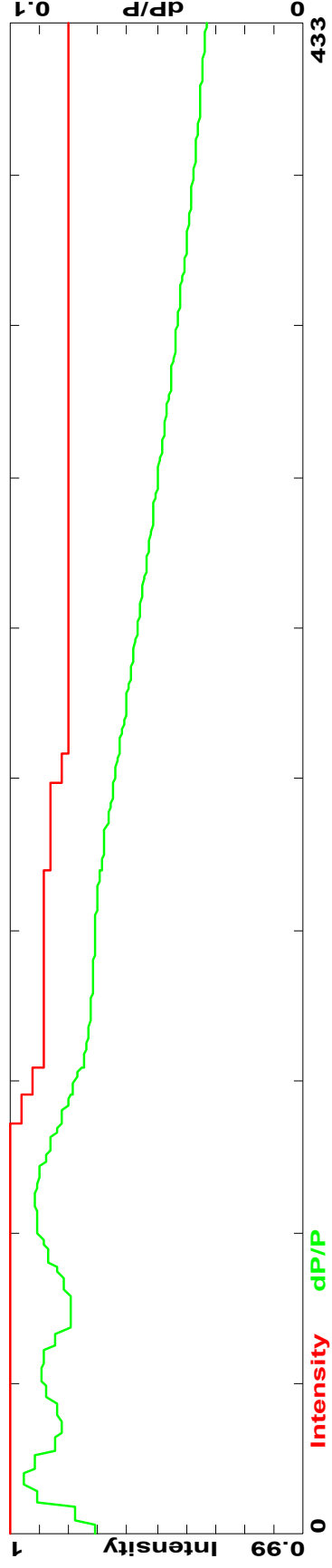


Figure 17. Longitudinal phase space at the beginning (left) and at the end (right) of the linac. Green crosses show particles lost in the course of acceleration.

Sat Feb 24 22:18:59 2001 OptiM - MAIN: - C:\Optics\NeutrinoFactory\Linac\Linac.opt



Sat Feb 24 22:19:47 2001 OptiM - MAIN: - C:\Optics\NeutrinoFactory\Linac\Linac.opt

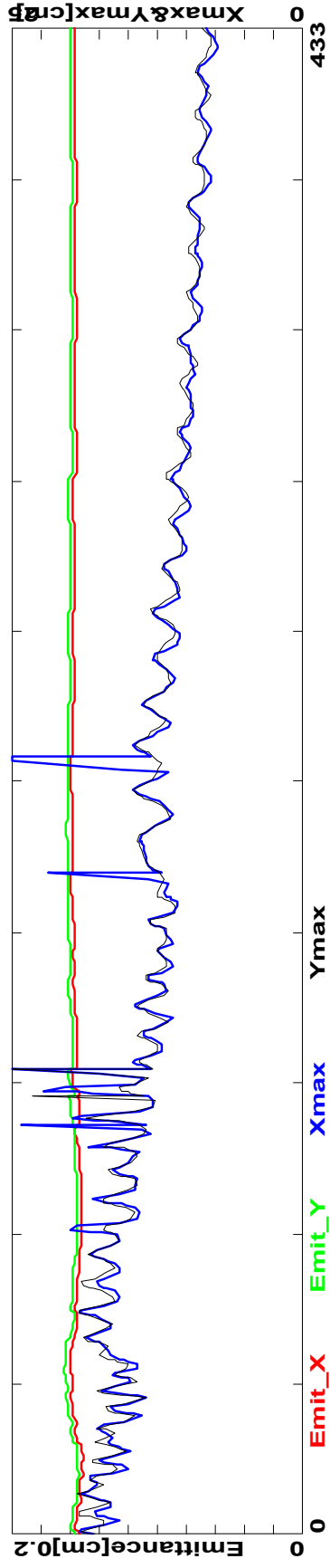


Figure 18. Dependence of beam intensity, rms momentum spread (top), beam emittances (normalized to the initial linac energy) and beam envelopes (bottom) along the linac.

1.4 Reinjection chicane

Reinjection chicane is used to inject the beam into recirculator. A simplified scheme of the chicane is presented in Figure 19. As one can see chicane is built from four dipoles and four quad triplets in between them to make chicane achromatic. The choice of standard three dipoles chicane cannot be used because the chicane has to be sufficiently long to bypass incoming higher energy arcs. Triplet focusing replaces solenoidal focusing used in the linac at the beginning of the chicane. An advantage of triplet focusing is that it has long straight sections necessary for beam separation at injection. Triplet focusing also naturally matches the solenoidal focusing. The period length is 15 m so that it would coincide with the period length of the downstream RLA linac. Betatron phase advance per cell is chosen to be 0.25. That is preferable from the point of view of chromatic effects compensation. Figure 20 depicts beta-functions, dispersions and beam envelopes in the chicane.

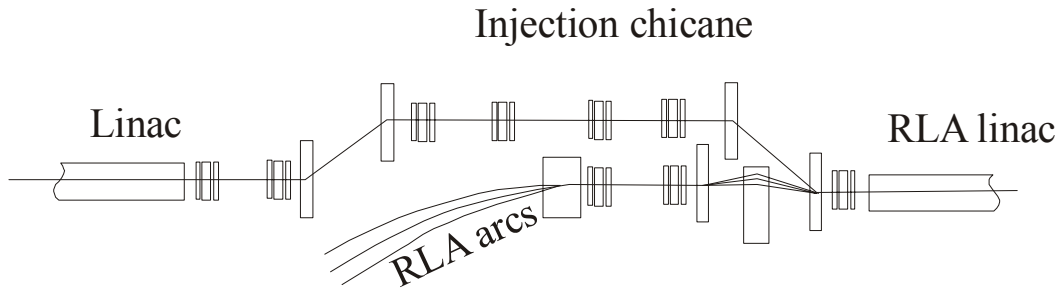


Figure 19. Scheme of reinjection chicane.

In the linac the chromatic effects are suppressed by periodicity of the focusing and does not require special correction. Unfortunately, it does not quite work when we introduce bends; and a sextupole chromatic correction is required for horizontal degree of freedom. It can be achieved by introducing sextupole component into the field of focusing quads of six triplets. Four of these quads are located at the top of the dispersion function for chromaticity compensation and the other two are located in front of the chicane for compensation of the non-linearity introduced by the chromaticity compensation quads as shown in Figure 20. Tracking studies showed that non-linearity of sextupole fields can be cancelled for comparatively small beam momentum spread but only limited cancellation can be achieved for about $\pm 10\%$ momentum spread corresponding to the momentum spread at the end of the linac (see Figure 17). Strong sextupole components required for good correction of second order dispersion cause too large emittance growth because of poor non-linearity cancellation and therefore a partial compensation of second order dispersion is preferable. In tracking studies values of all six sextupole components were varied independently to minimize overall emittance growth through the chicane. It was found that if all sextupole components are proportional to corresponding quadrupole components (preferable technical choice) the emittance growth is close to its minimum value. Such a choice required only one additional type of quadrupoles and therefore it was adopted. Optimal ratio of sextupole and quadrupole components is $S/G = 0.00355 \text{ cm}^{-1}$. That corresponds to 7% correction of quadrupole gradient at radius of 20 cm. Figure 21 depicts the beam envelopes and the beam emittance normalized to the initial linac energy, $\epsilon\gamma\beta/\gamma_0\beta_0$. As one can see the

horizontal emittance grows by 13% and the vertical one by 3% with no loss. Maximum horizontal beam size is achieved at the last chicane triplet and equal to ± 19 cm.

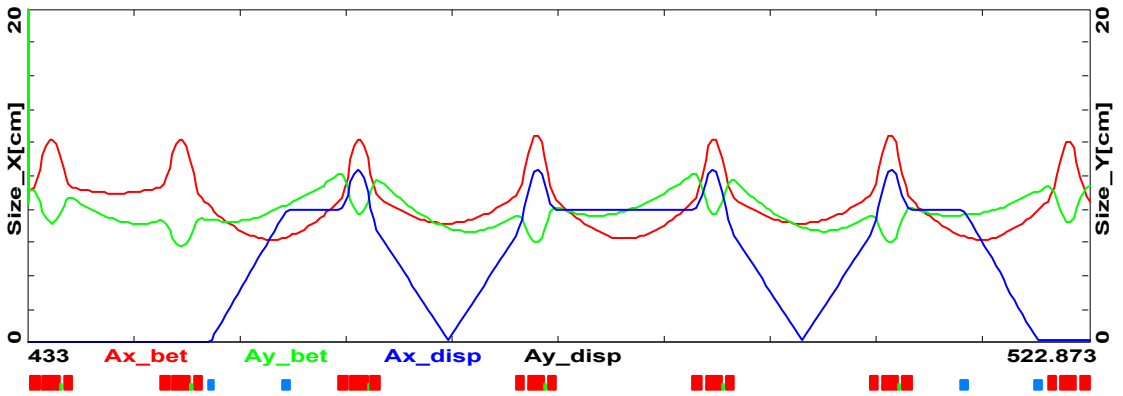
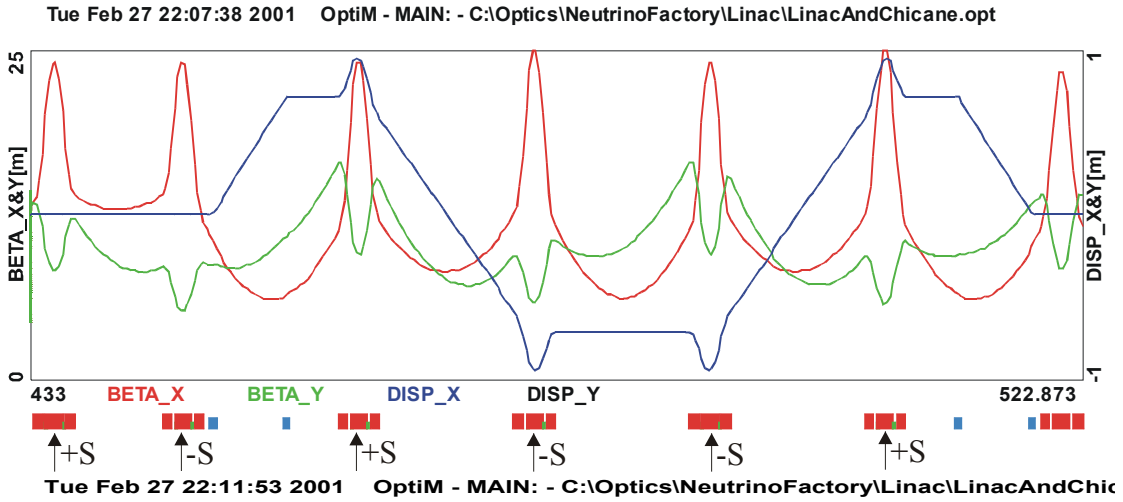


Figure 20. Beta-functions, dispersions (top plot) and beam envelopes (bottom plot) in the chicane.

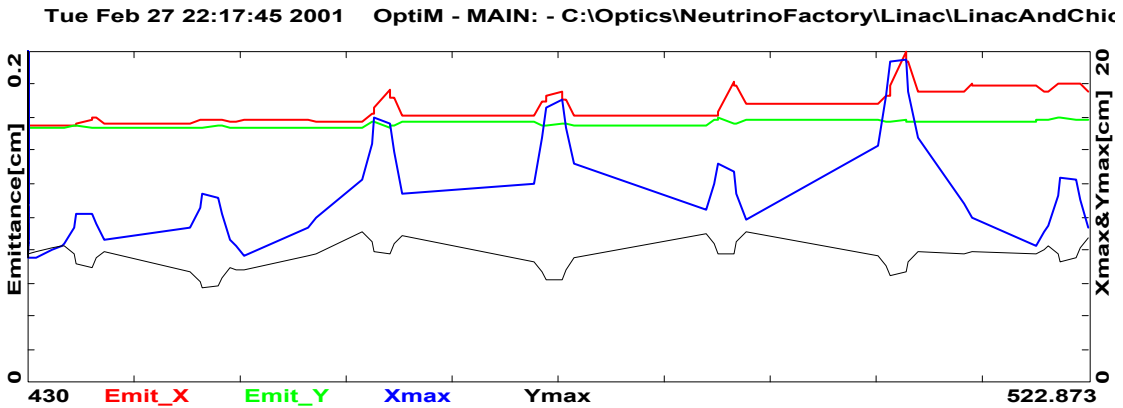


Figure 21. Dependence of beam emittances (normalized to the initial linac energy) and beam envelopes along the linac.

Figure 22 shows the injector chicane in vicinity of the separation point. To minimize emittance growth the angle of the chicane dipoles is chosen to be as small as possible. The separation is determined by the beam sizes and the space required for the septum

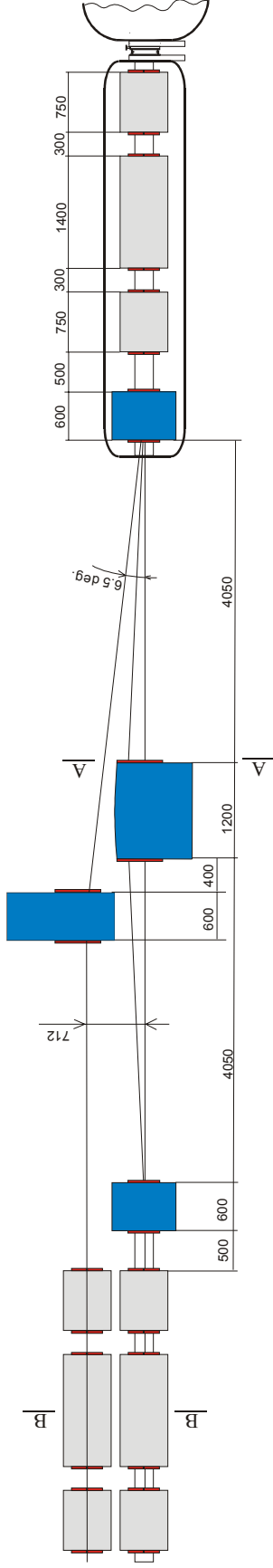


Figure 23. Layout of injection chicane at separation point

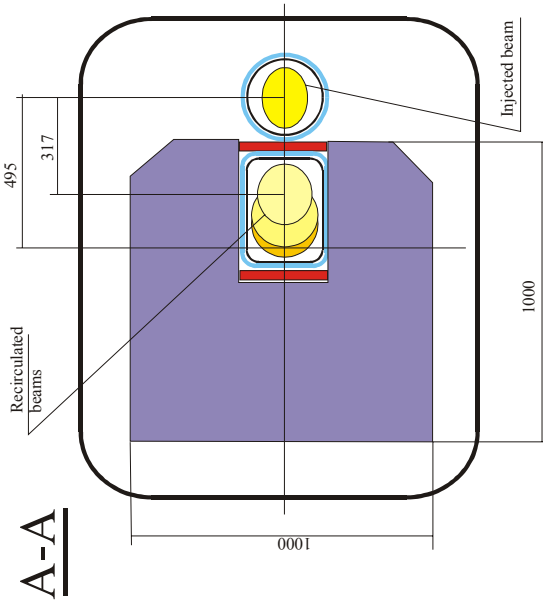


Figure 24. Cross section of injection chicane at the separation point

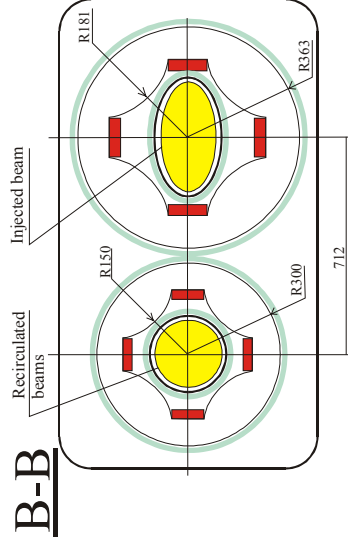


Figure 25. Cross section of injection chicane at a focusing quad

magnet coil. Figure 24 and 25 show cross sections of injector chicane at the separation point and in the center of focusing quad. Taking into account large apertures of magnets (~ 30 cm) and their comparatively modest magnetic fields (<2 T) it looks preferable to use magnets with SC coils and the field formed by the magnetic core. Currently we presume that steel is also cooled to liquid helium temperature. Such choice allows one to get compact magnets and significantly reduce required power. Tables 4 and 5 present parameters of dipoles and quadrupoles for the injection chicane.

Table 4. Parameters of injection chicane quads

	Number of magnets	Maximum gradient [T/m]	Length [m]	Aperture [m]	Built-in sextupole, S/G [m ⁻¹]
Focusing quad	3	4	1.40	0.15	0
Defocusing quad	14	4	0.75	0.15	0
Large aperture quad	4	4	1.40	0.181	0.355

Table 5. Parameters of injection chicane dipoles

	Number of magnets	Maximum field [T]	Length [m]	Gap [m]	Width
Short dipole	4	1.7	0.6	0.30	0.30
Long septum	1	1.7	1.2	0.30	0.38
Short septum	1	1.7	0.6	0.30	0.38

2. Recirculating Linac(RLA)

2.1 Longitudinal dynamics in recirculating linac

Bunch length and energy spread are still too large at the RLA input and their further compression is required in the course of acceleration. To achieve this the beam is accelerated off-crest with non zero M_{56} (momentum compaction). That causes synchrotron motion, which suppresses the longitudinal emittance growth related to non-linearity of accelerating voltage. Without synchrotron motion the minimum beam energy spread would be determined by non-linearity of RF voltage at bunch length and would be equal to $(1-\cos\phi) \approx 6\%$ for bunch length $\phi=20$ deg. The synchrotron motion causes particle motion within the bunch and averages the total energy gain of tail's particle to the energy gain of particles in the core. The parameters of acceleration are presented in Table 6 and corresponding boundaries of longitudinal phase space are presented in Figure 26. It was chosen to have the same (or at least close) M_{56} for all arcs. The optimum value is about 1.4 m, while optimal detuning of RF phase from on-crest position is different for different arcs. As one can see although longitudinal motion is still quite non-linear it is possible to reduce the energy spread by 4.7 times to $\pm 1.6\%$ with emittance dilution of about 75%. In these calculations targeted to be the design intent for arc optics we presume that the longitudinal displacement is the function of momentum only² and it is its linear function, $\Delta L/L = M_{56} \Delta p/p$. The horizontal and vertical acceptances of arcs in Table 6 are presented with emittance dilutions of 9% and 4% per arc. Such a choice is supported by preliminary tracking results. Final details of beam dynamics depend on the

² Additional correction can come from particle transverse oscillation and non-linear dispersion.

beam transport optics and can be only determined by tracking discussed below.

Table 6. Parameters for acceleration in the recirculator

	Kinetic energy [GeV]	Gang phase [deg]	Total energy spread, $2\Delta p/p$ [%]	Horizontal acceptance, [mm mrad]	Vertical acceptance, [mm mrad]
Entrance	2.480	0	15.0	669	638
Arc 1	4.756	-23	11.3	384	350
Arc 2	6.884	-23	8.9	292	253
Arc 3	9.017	-23	6.7	244	202
Arc 4	11.150	-23	5.8		

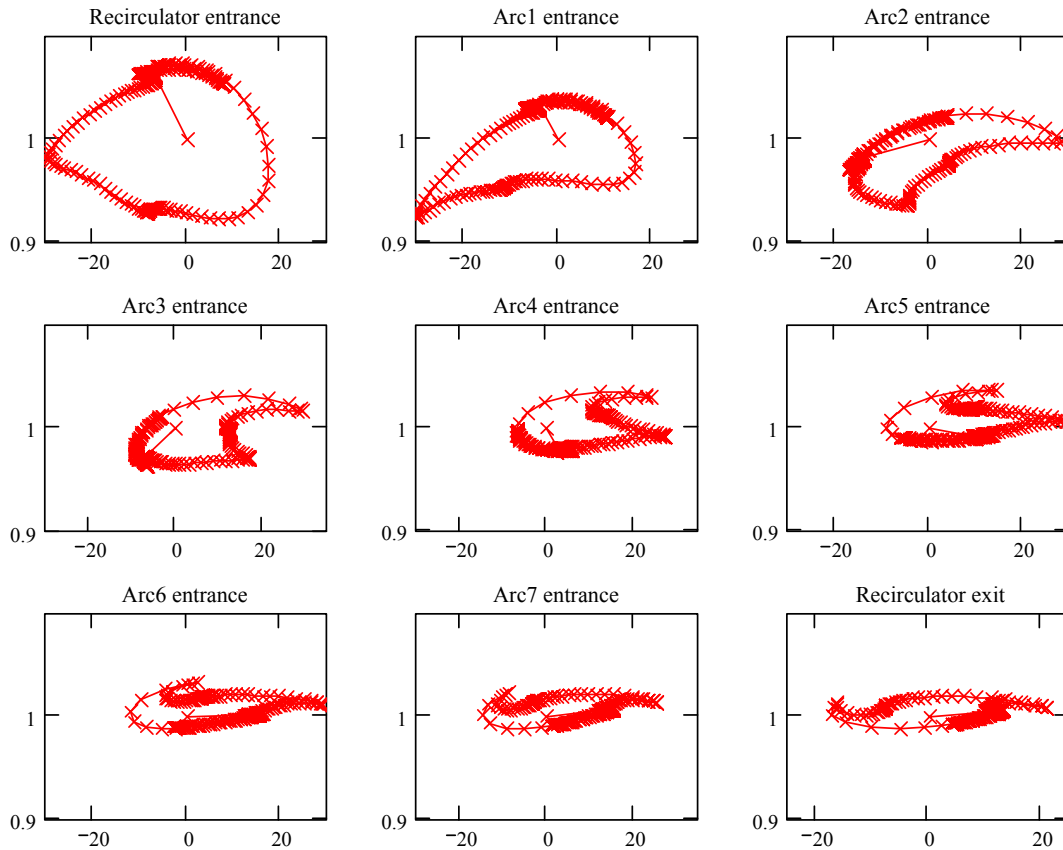


Figure 26. Boundaries of the beam longitudinal phase space at different locations in the recirculator; $M_{56}=1.4$ m.

The beam intensity is high and the beam loading has to be taken into account. It causes the RF voltage droop by $\sim 0.6\%$ per pass yielding $\sim 2.4\%$ loss in acceleration for the tail bunch of the last pass. It is comparable with energy aperture of high arcs and their optics tuning has to be done with energy droop taken into account. Another worry is that the first and the last bunches see different accelerating voltage and experience different longitudinal dynamics. Fortunately, accelerating off-crest resolves this problem as well.

In this case, after acceleration in the first linac, the last bunch experiences less acceleration; but then because of smaller energy the bunch comes faster through the first arc and is accelerated with smaller RF phase causing higher acceleration in the next linac. In other words the bunch center of the last bunch experiences synchrotron motion relative to the center of first bunch. That suppresses the effect of accelerating voltage droop. Figure 27 shows longitudinal phase space for the first and the last bunches at the end of accelerator.

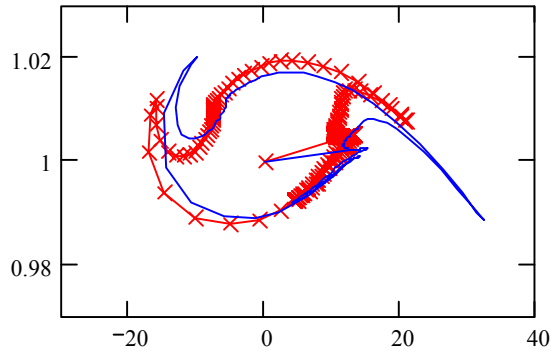


Figure 27. Boundaries of the beam longitudinal phase space at the end of recirculator for the first bunch (line with crosses) and the last bunch (solid line); $M_{56} = 1.4$ m, energy droop of 0.6% per pass corresponding to $3 \cdot 10^{12}$ particle train

The acceleration has been optimized so that the energy spread of both bunches would be the same. One can see that the beam loading significantly changes the bunch shape but the energy droop cannot be seen.

2.2 General parameters and period layout of RLA linac

Both RLA linacs have the same period. The period consists of a cryo-module with four SC cavities and a cryo-module with quad triplet. Period layout is presented in Figure 28. Design and parameters of the cavities are the same as for the cavities of long cryo-module of linac preaccelerator (see Table 3). In distinguish of linac-preaccelerator, having just one cryo-module per period, the linac period has separate cryo-modules for cavities and triplets. It is preferred due to longer length of the period. The design and parameters of triplets of the first RLA linac is similar to the small triplets of injection chicane with higher accelerating gradient ranging from 3.2 to 6.7 T/m. The quadrupoles of the second RLA linac have similar design with 1.5 times smaller aperture equal to 100 mm. Their accelerating gradient ranges from 6.2 to 9.7 T/m.

Figures 29 - 30 show the beta-functions and beam envelopes for the first and the last passes in the first RLA linac. Beta-functions of the first pass for the second RLA are the same as for the first RLA. The last pass beta-functions of the second RLA are smaller then the corresponding beta-functions of the first RLA because of smaller energy difference for the last and the first passes. Figure 31 shows the beam envelopes for the first and the last passes in the second RLA linac. The difference between the vertical and horizontal beam sizes for the last pass is related to a larger horizontal emittance determined by higher horizontal emittance growth. The focusing structure for the both linacs is chosen so that to have the same betatron phase advance per cell for the first pass beam. The requirement to have similar horizontal and vertical beta-functions for the higher passes determines that the horizontal and vertical phase advances are not equal. Figure 32 shows the line on the tune diagram where the horizontals and vertical beta-functions are approximately equal for the last pass of the first linac. Parameters of linac periods are presented in Table 7.

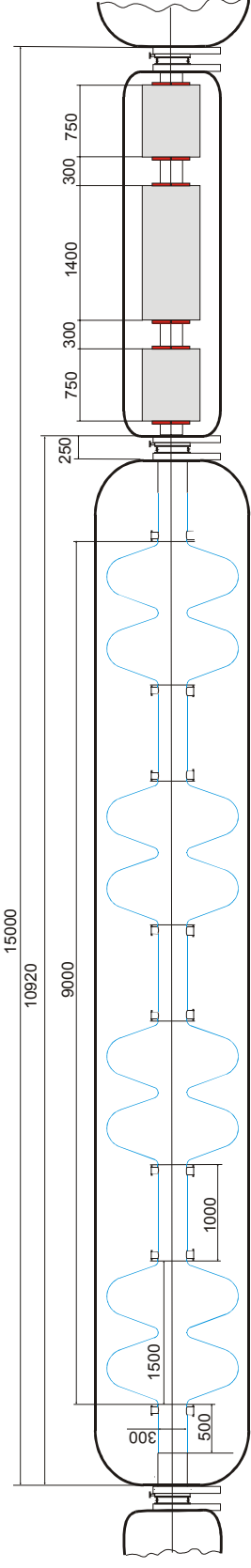
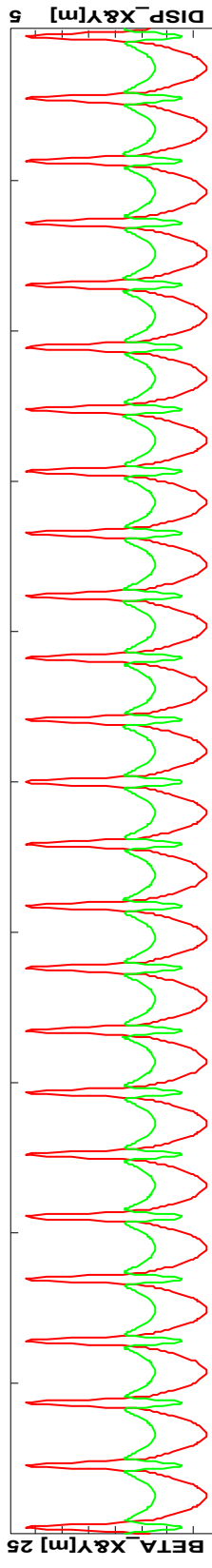
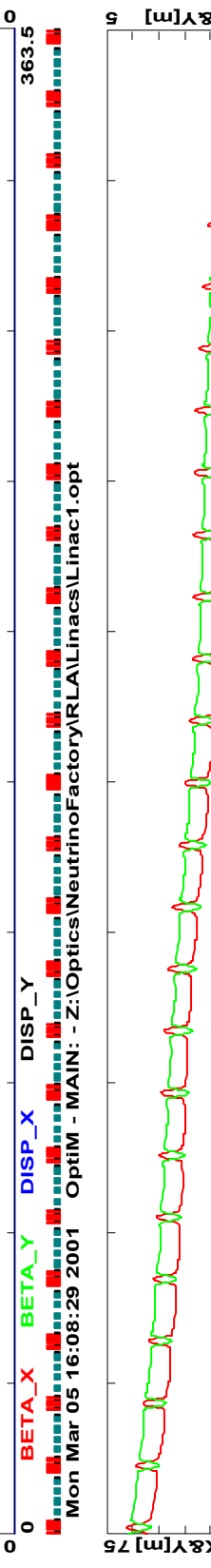


Figure 28. Layout of RLA linac period.

Mon Mar 05 16:08:15 2001 OptiM - MAIN: - Z:\Optics\NeutrinoFactory\RLA\Linacs\Linac1.opt



Mon Mar 05 16:08:29 2001 OptiM - MAIN: - Z:\Optics\NeutrinoFactory\RLA\Linacs\Linac1.opt



Mon Mar 05 16:08:29 2001 OptiM - MAIN: - Z:\Optics\NeutrinoFactory\RLA\Linacs\Linac1.opt

Figure 29. Beta-functions for the first (top) and the last (bottom) pass of the first RLA linac.

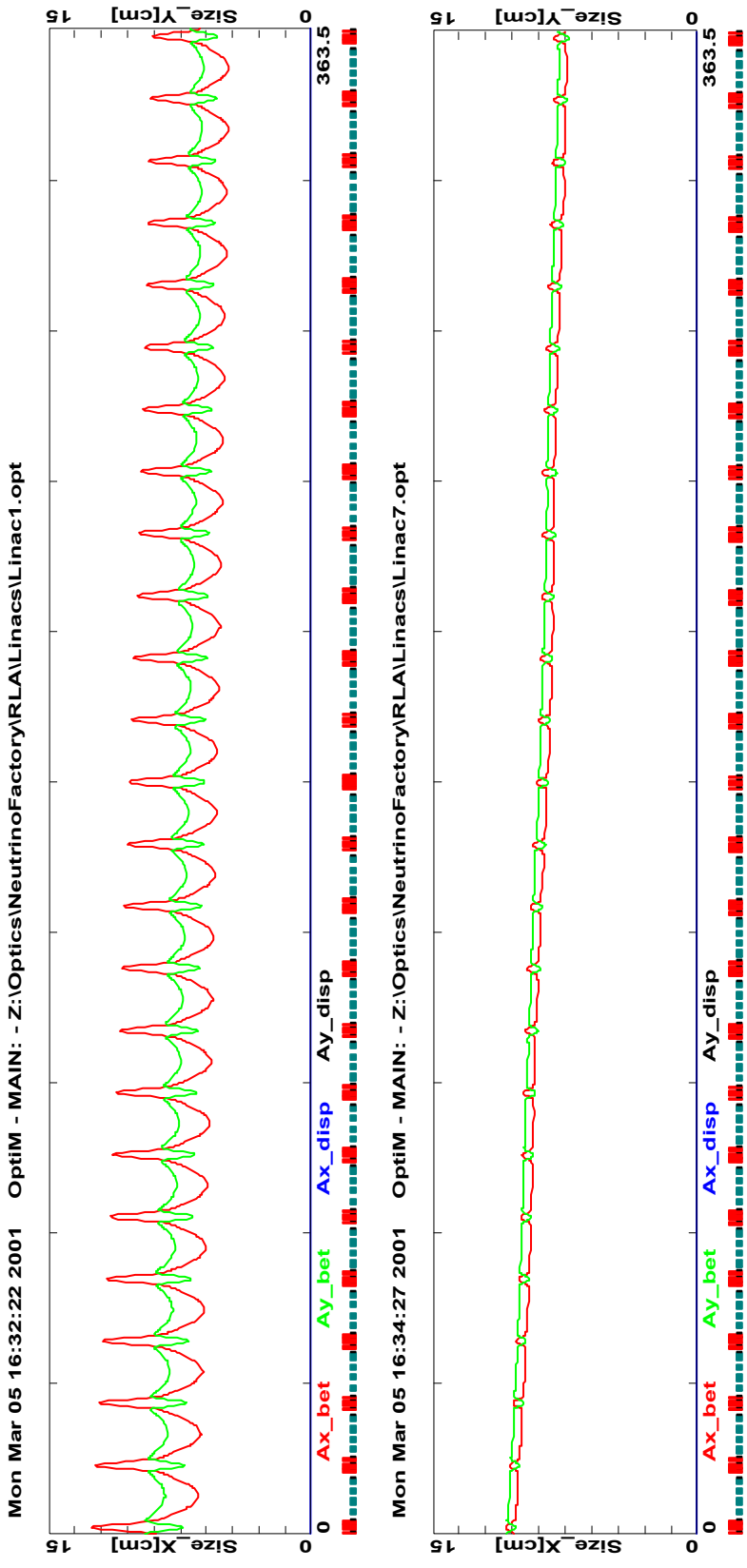


Figure 30. Beam envelopes for the first (top) and the last (bottom) pass of the first RLA linac.

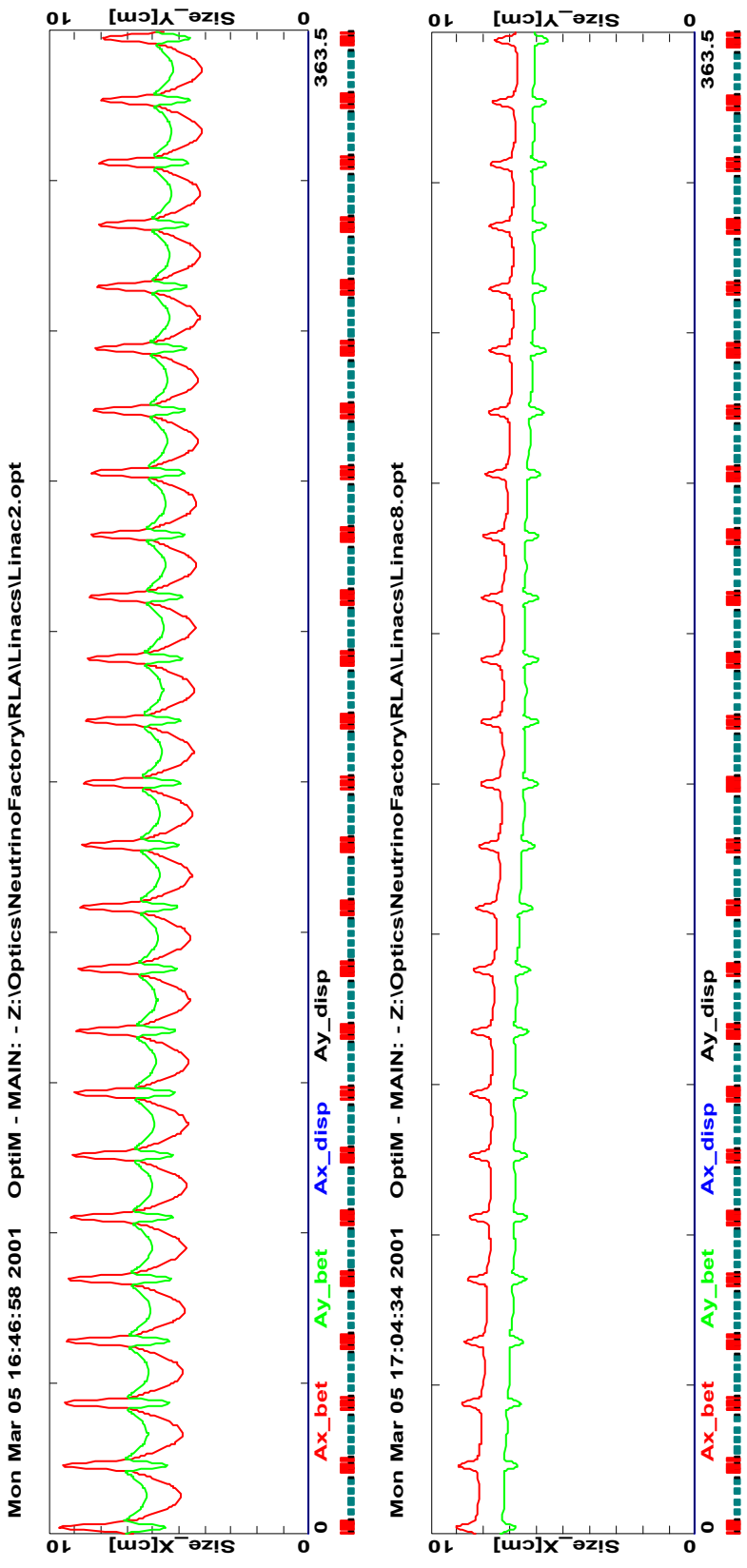


Figure 3.1. Beam envelopes for the first (top) and the last (bottom) pass of the second RLA linac.

Table 7. Parameters of the RLA linac periods

	Linac 1	Linac 2
Number of periods	24	24
Total length of one period	15 m	18 m
Number of cavities per period	4	4
Number of cells per cavity	2	2
Number of couplers per cavity	2	2
Cavity accelerating gradient	17 MV/m	17 MV/m
Aperture in cavities ($2a$)	300 mm	300 mm
Aperture of quadrupole ($2a$)	300 mm	200 mm
Focusing quad length	1.4 m	1.4 m
Defocusing quad length	0.75 m	0.75 m
Quadrupole gradient	3.2-6.7 T/m	6.2-9.7 T/m

Each cavity cryo-module has vacuum valves at both ends and is delivered to the tunnel under vacuum. These valves are slow and, currently, it is not feasible to build a sufficiently fast valve to prevent major vacuum failures in a vacuum chamber of so large aperture. Therefore each linac is separated from arcs with 0.5 mm beryllium windows. It also resolves the question of differential pumping between high vacuum in RLA linacs and low vacuum in arcs, which otherwise would be a major issue for vacuum chamber of such aperture. The design and size of windows are similar to the beryllium windows used for the ionization cooling. Altogether there are 5 windows: one in the injection chicane, and four at both ends of both RLA linacs. Multiple scattering causes the total emittance growth of about 5% for windows of 0.5 mm thickness. The contribution into emittance growth from different passages through windows is almost even: the beam of higher energy experiences smaller scattering but it has proportionally larger beta-function in multipass linacs.

2.3 Beam dynamics in the RLA linacs

To choose a working point we took into account the following considerations. First, due to symmetry of quadrupole field the lowest non-linearity of its fields has sixth order and therefore one would like to be far away from sixth order resonances. Second the beam size should be close to its minimum for given period length; and third, the chromaticity of beam envelopes should be minimized. The chosen tunes of $Q_x=0.273$, $Q_y=0.204$ satisfy the above requirements. For higher passes the tune advance per cell is not constant and grows from the beginning to the end of the linac. That causes the tune to cross a few resonances. The most sensitive is the second pass, which tunes cross the sixth order resonances. Nevertheless the tracking exhibited that all higher passes are less sensitive to quad non-linearity than the first pass. The first RLA linac is more sensitive to quads non-linearity because of larger beam size for all passes. Therefore it sets the limit for acceptable quadrupole non-linearity. For simulations we assumed that non-linear terms are proportional to the quadrupole gradients. The non-linearity is described by parameter

$$F_n = \frac{1}{Ga} \frac{a^{n-1} B_n}{n!} \quad , \quad (3)$$

which determines a relative correction of the gradient at the reference radius a . Table 8

summarizes results of simulations performed for the first RLA linac. The data are shown for the reference radius of 10 cm, which is close to the beam envelope in the focusing quads. As one can see the requirements for quadrupole non-linearity are very modest. Summarizing we can conclude that the accuracy of quadrupole field integral better than 1% at the reference aperture of 100 mm aperture is sufficient. With such presumption tracking in the linacs did not exhibit any significant emittance growth which as will be seen below happens in arcs where periodicity of motion is broken.

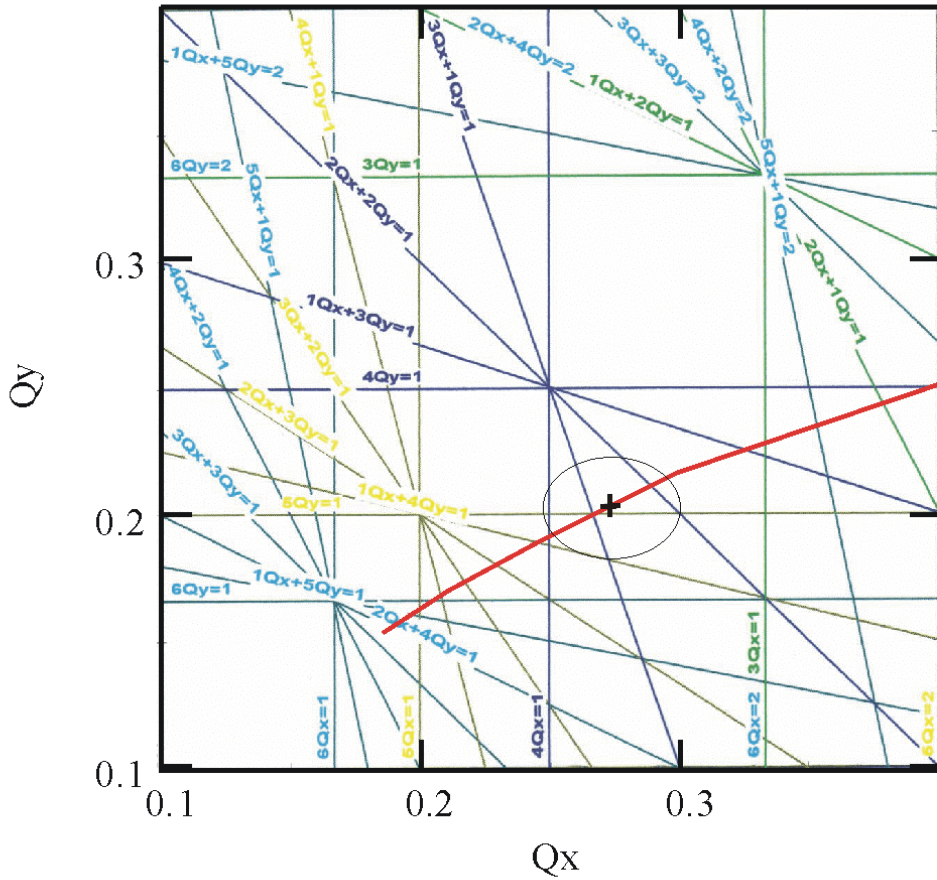


Figure 32. Tune diagram for 1 period of the first pass in RLA linac. Solid line shows tunes where $\beta_x = \beta_y$ for the highest energy pass. The cross shows the chosen tune, $Q_x=0.273$, $Q_y=0.204$, and the circle around it corresponds to the tune changes corresponding to 10% energy spread.

Table 8. Acceptable non-linear fields of quadrupoles

	4-th order (octupole)	6-th order	10-th order
$ F_n $	< 0.015	< 0.02	< 0.02

As it was already mentioned there is a significant RF phase slip for the beam at different passes because of different particle velocities at different energies. Figure 33 presents RF phases for the beam at different passes assuming that the cavity phases set so that the second pass beam would be on crest. One can see that the first pass beam of the first RLA linac has phase variations in the range of -19 to 12 deg. That reduces its

effective accelerating gradient by 1.2% but it does not produce any significant effect for higher passes.

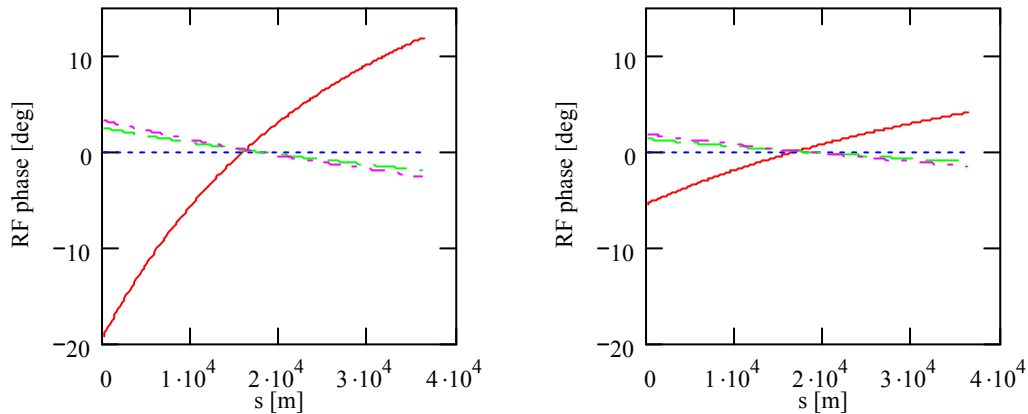


Figure 32. RF phase for different passes through the first (left) and second (right) RLA linacs. Solid line – pass 1, dotted line – pass 2, dashed line – pass 3, and dot-dashed line – pass 4.

2.4 Arcs, spreaders and recombiners

The RLA beam transport system uses a horizontal separation of beams at the end of each linac to allow independent recirculation of each pass. Individual recirculation arcs are based on a periodic triplet focusing structure, which is a smooth continuation of linac focusing. The period length is slightly shorter than for the linacs to achieve desired small value of M_{56} . The triplet focusing has a few advantages in comparison with FODO focusing. First, it has larger distance between quads, which significantly simplifies spreader/recombiner design. Spreading and recombining the beams with FODO lattice is going to be much more complicated if possible at all. Second, it allows simple and smooth beam envelop matching from linac to recirculation arc, which is very important for the beams with considered energy spread. Third, the triplet focusing has twice smaller chromaticity of vertical beam envelope in comparison with FODO focusing and requires chromatic corrections only for horizontal degree of freedom.

The required large momentum acceptance necessitates introduction of a three-sextupole family chromatic correction of the off-momentum orbit and path length. As in other recirculating linacs, and unlike storage rings and synchrotrons, correction of betatron “tunes” is unnecessary. Figure 33 shows a spreader (recombiner) layout.

Has to be covered in Hasan's contribution

RF considerations

Peak power is then determined by microphonics [4] leading to a choice of long pulse operation of the RF cavities and reducing total power consumption for both RF and cryogenics. The final issue represents the traditional beam dynamics concerns associated with any high brightness accelerator. A very preliminary study suggests that the beam stability is not expected to be a severe problem [5] and will not be further discussed in this article.